HHS Public Access

Author manuscript

Nature. Author manuscript; available in PMC 2015 July 29.

Published in final edited form as:

Nature. 2015 January 29; 517(7536): 635–639. doi:10.1038/nature13886.

Uncovering the Polymerase-induced Cytotoxicty of an Oxidized Nucleotide

Bret D. Freudenthal[1], **William A. Beard**[1], **Lalith Perera**[1], **David D. Shock**[1], **Taejin Kim**[2], **Tamar Schlick**[2], and **Samuel H. Wilson**[1,*]

[1]Laboratory of Structural Biology, National Institute of Environmental Health Sciences, NIH, P.O. Box 12233, Research Triangle Park, North Carolina 27709-2233, USA.

[2]Department of Chemistry and Courant Institute of Mathematical Sciences, New York University, 251 Mercer Street, New York, New York 10012, USA.

Abstract

Oxidative stress promotes genomic instability and human diseases[1]. A common oxidized nucleoside is 8-oxo-7,8-dihydro-2'-deoxyguanosine found both in DNA (8-oxo-G) and as a free nucleotide (8-oxo-dGTP)[2,3]. Nucleotide pools are especially vulnerable to oxidative damage[4]. Therefore cells encode an enzyme (MutT/MTH1) that removes free oxidized nucleotides. This cleansing function is required for cancer cell survival[5,6] and to modulate *E. coli* antibiotic sensitivity in a DNA polymerase (pol)-dependent manner[7]. How polymerase discriminates between damaged and non-damaged nucleotides is not well understood. This analysis is essential given the role of oxidized nucleotides in mutagenesis, cancer therapeutics, and bacterial antibiotics[8]. Even with cellular sanitizing activities, nucleotide pools contain enough 8-oxo-dGTP to promote mutagenesis[9,10]. This arises from the dual coding potential where 8-oxo-dGTP*(anti)* base pairs with cytosine (Cy) and 8-oxodGTP*(syn)* utilizes its Hoogsteen edge to base pair with adenine (Ad)[11]. Here we utilized time-lapse crystallography to follow 8-oxo-dGTP insertion opposite Ad or Cy with human DNA pol β, to reveal that insertion is accommodated in either the *syn*- or *anti*-conformation, respectively. For 8-oxo-dGTP*(anti)* insertion, a novel divalent metal relieves repulsive interactions between the adducted guanine base and the triphosphate of the oxidized nucleotide. With either templating base, hydrogen bonding interactions between the bases are lost as the enzyme reopens after catalysis, leading to a cytotoxic nicked DNA repair intermediate. Combining structural snapshots with kinetic and computational analysis reveals how 8-oxodGTP utilizes charge modulation during insertion that can lead to a blocked DNA repair intermediate.

*Correspondence to: wilson5@niehs.nih.gov.

Author Contributions B.F, W.B., and S.W. designed the project. B.F. carried out crystallography. D.S. did the kinetic analyses. T.K. and T.S did the molecular dynamics simulations. L.P. did the quantum mechanical analysis. B.F., W.B., and S.W. prepared the manuscript. All authors discussed the results and commented on the manuscript.

The authors declare no competing financial interests. Atomic coordinates and structure factors for the reported crystal structures have been deposited with the Protein Data Bank with accession codes 4UAW, 4UA(Y-Z), 4UB(1-5), 4UB(B-C). Readers are welcome to comment on the online version of this article at www.nature.com/nature.

A primary defense mechanism against oxidative DNA damage is base excision repair, which in eukaryotes utilizes pol β[12,13]. During times of oxidative stress, pol β can perform futile repair by inserting 8-oxo-dGTP opposite Cy or Ad (Fig. 1a-c), and it is implicated in driving tumorigenesis[14,15]. Pol β binds to gapped DNA in an open conformation; upon binding the incoming nucleotide it undergoes a conformational change to form the pre-catalytic closed complex with two active site divalent metals ions: the catalytic (Mg_c) and nucleotide (Mg_n) metals[16-18]. This complex is optimized for nucleotidyl transfer, forming pyrophosphate (PP_i), and following catalysis, pol β reopens, releasing PP_i.

Soaking open binary crystals of pol β bound to DNA containing a templating Ad in a cryosolution with 8-oxo-dGTP and $CaCl_2$ results in a closed pre-catalytic ground state (GS) ternary complex (Extended Data Table 1). The incoming 8-oxo-dGTP(*syn)* Hoogsteen base pairs with Ad (Fig. 1d). The active site is in a similar conformation as previously observed using a dideoxy-terminated primer (Extended Data Fig. 1a)[19], with a change in the primer terminus sugar pucker to C3'-endo (Extended Data Table 2). Unique active site interactions include Asn279 hydrogen bonding to O8 of 8-oxo-dGTP(*syn)* and an intramolecular hydrogen bond between N2 and the pro-S_p oxygen on Pα of 8-oxodGTP(*syn*) (Fig. 1d). This is consistent with previous studies identifying a role of Asn279 in stabilizing 8-oxo-dGTP*(syn)*[20].

To observe catalysis the GS crystals were transferred to a solution containing $MgCl_2$ for 20 s (Extended Data Table 1). Density corresponding to both the reactant and product was observed (Fig. 1e and Extended Data Fig. 1b) and based on occupancy refinement the reaction is 60% "complete". In comparison to the GS there is only moderate movement in the active site, at Pα and O3' (Extended Data Fig. 1b-c). The Hoogsteen base pairing and hydrogen bonding interactions that stabilize the planar *syn*conformation are maintained, and the enzyme remains in the closed conformation. These observations are consistent with 8-oxo-dGTP insertion opposite Ad exhibiting a high catalytic efficiency (Fig. 1c).

Extending the $MgCl_2$ soak time to 40 s resulted in complete turnover of the reactant 8-oxo-dGTP*(syn)* in the closed polymerase conformation (Extended Data Table 1 and Fig. 1f). This post-chemistry complex shows the Hoogsteen base pairing and the intramolecular hydrogen bond at N2 are maintained, and Asn279 hydrogen bonds with O8. The catalytic Mg^{2+} has been replaced by Na^+, while the nucleotide Mg^{2+} remains in the active site coordinating PP_i (Extended Data Fig. 1d-e). The closed product complex contains a new Mg^{2+} product metal (Mg_p) that bridges the backbone phosphate of 8-oxodGMP *(syn)* and PP_i.

Extending the $MgCl_2$ soak to 90 s results in a closed-to-open conformational change (Fig. 1g). The PP_i and associated metals have disassociated, and the inserted 8-oxo-dGMP *(anti)* has lost the interaction between Asn279 and O8, promoting destabilization of the Hoogsteen base pairing. The inserted 8-oxo-dGMP has a high B-factor (57 $Å^2$; Extended Data Table 1), with the most stable position displaced into the major groove and a weak hydrogen bond formed between N6 of Ad and N3 of 8-oxodGMP (Extended Data Fig. 1f).

The insertion efficiency of 8-oxo-dGTP opposite Cy is much less than opposite Ad (Fig. 1c); this may arise from a clash between O8 and Pα of 8-oxo-dGTP*(anti)* (Fig. 1a)[19,21]. To probe

how this clash is accommodated we soaked open binary pol β complex crystals with a templating Cy in a cryosolution containing 8-oxo-dGTP/$CaCl_2$. The resulting closed ternary GS complex contains 8-oxo-dGTP*(anti)* Watson-Crick base pairing with the templating Cy (Extended Data Table 3 and Fig. 2a). The clash at O8 is partially eased by an altered sugar pucker, glycosidic angle, buckle, and shear compared to dGTP*(anti)* (Extended Data Table 2). The incoming 8-oxo-dGTP*(anti)* N3 and N2 atoms are within hydrogen bonding distance of Asn279 and Arg283, respectively (Fig. 2b). To determine if these are unique contacts we solved the structure of dGTP*(anti)* Watson-Crick base pairing with Cy in the presence of $CaCl_2$ (Extended Data Table 3). Comparing these two structures indicates the contact with Arg283 may be unique to the incoming 8-oxo-dGTP*(anti)* because O8 causes the triphosphate and base to move 1.1 Å apart (Fig. 2c). This shift promotes the phosphate backbone of Cy to move 2.6 Å into the minor groove (Fig. 2b). Mutating Arg283 to lysine or alanine reduced the 8-oxo-dGTP specificity from favoring 8-oxo-dGTP(*syn*) insertion opposite Ad by 40-fold for wild-type, to six-fold and two-fold for the R283K and R283A mutants, respectively (Fig. 2d). This loss of discrimination against insertion of 8-oxo-dGTP*(anti)* opposite Cy indicates Arg283 promotes the mutagenic insertion of 8-oxo-dGTP*(syn)* by acting as a steric gate to prevent insertion opposite Cy. Interestingly, during the bypass of 8-oxo-G in the templating position, Arg283 stabilizes the mutagenic *syn*-conformation[22].

The changes described above do not fully alleviate the clash between O8 and the sugar-phosphate backbone of the incoming 8-oxo-dGTP(*anti*) (red dashes in Fig. 2b). Surprisingly, this clash is accommodated by an additional divalent metal (Ca_g) observed coordinating the pro-S_p oxygen of Pα and five water molecules (Fig. 2a-b). Two of the water molecules are also within hydrogen bonding distance of O8 (Fig. 2b). To verify the presence of this additional divalent metal binding site near Pα, we soaked the closed pre-catalytic GS complex (8-oxo-dGTP:Cy) in $MnCl_2$ for 5 s (Extended Data Table 3). This allows metal exchange before catalysis had appreciatively occurred (Extended Data Fig. 2a). The presence of Mn^{2+} in the catalytic, nucleotide, and ground state sites was verified by anomalous density. Overlaying the GS complex with Ca^{2+} and Mn^{2+} verified the ground state metal site binds divalent cations (Extended Data Fig. 2b).

To observe 8-oxo-dGTP*(anti)* insertion we soaked a GS crystal in $MgCl_2$ for 40 s (Extended Data Table 3). Pol β remained in the closed conformation with density corresponding to both product and reactant species (Fig. 2e). Occupancy refinement indicates the reaction is 40% complete. The Watson-Crick base pairing interactions are maintained with only moderate movement at the reacting atoms (Pα and O3'; Fig. 2e). The phosphate backbone of the templating Cy is observed in two conformations corresponding to reactant and product. Surprisingly, density for both ground state and product metals can be observed, indicating there are two distinct populations within the crystal (Extended Data Fig. 3).

Soaking pre-catalytic complex crystals in $MgCl_2$ for 60 s results in a closed product complex (Extended Data Table 3). 8-oxo-dGTP(*anti)* has been completely inserted with the sugar pucker shifting from a C4'-exo (GS) to C3'-endo (Extended Data Table 2 and Fig. 3a). Importantly, there is no density corresponding to the GS metal and only the product-associated metal is present (Fig. 3a-b). The clash at O8 has not been fully alleviated in the

product complex and is likely being mediated by the product Mg^{2+} (Fig. 3c). Overlaying the closed ground (0 s) and product states (60 s) indicates that ground state and product metal binding sites are in distinct positions separated by 2.0 Å that are dependent on having either substrate or product present (Fig. 3d). Extending the soak time in $MgCl_2$ to 120 s resulted in pol β transitioning to an open conformation (Extended Data Table 3). Watson-Crick base pairing is lost, 8-oxo-dGMP stacks over the templating base with a high B-factor (65.2 $Å^2$), and the remaining PP_i and associated metals have dissociated (Fig. 3e).

Quantum mechanical analysis allows the point charge on each atom of dGTP*(anti)* and 8-oxo-dGTP*(anti)* to be calculated (Extended Data Table 4 and Extended Data Fig. 4). Figure 4a illustrates the charge difference between 8-oxo-dGTP and dGTP mapped onto each atom of dGTP. The adducted O8 causes the oxygen bridging the sugar moiety and triphosphate (O5) to become more positive. Likewise, the pro-S_p oxygen of Pα becomes more negative and may facilitate recruitment of the GS metal. We also calculated the charge on each atom of 8-oxo-dGTP*(anti)* with all three metals (Extended Data Table 4 and Extended Data Fig. 4). Figure 4b shows the difference in charge of 8-oxo-dGTP*(anti)* with three metals from that with two metals (Ca_c and Ca_n) mapped onto the structure of 8-oxo-dGTP*(anti)*. The largest electronegative change is localized on the triphosphate at key catalytic atoms. This includes making Pα and Pβ more positive, while their bridging oxygen becomes more negative.

Molecular dynamics (MD) simulations using the pre-catalytic 8-oxo-dGTP*(anti)* or dGTP*(anti)* opposite Cy structures indicate a stable Mg_g coordination sphere (Extended Data Table 5). With 8-oxo-dGTP*(anti)*, one of the Mg_g-coordinating water molecules forms a hydrogen bond with O8, while the inter-atomic distances in the active site maintain proper catalytic values (Extended Data Fig. 5a-b). In comparison, the dGTP*(anti)* system exhibits poor geometry. The average distance of Pα-O3' increases to 5.25 ± 1.0 Å (Extended Data Fig. 5c), and the coordination between Mg_c and O3' is broken due to a newly established coordination network with another water molecule at 40 ns. All these events in the dGTP*(anti)* system induce larger RMSD than those of 8-oxo-dGTP*(anti)* system when the evolving MD system is compared to the initial structure, indicating that Mg_g in the dGTP*(anti)* is less favorable and associated with a much less competent-for-chemistry geometry compared to the 8-oxo-dGTP*(anti)* system (Extended Data Fig. 5c-d).

Interestingly, we captured 8-oxo-dGTP*(anti)* Watson-Crick base pairing in a nearly identical manner to that observed for dGTP*(anti)*. This required recruitment of an additional divalent metal near Pα of 8-oxo-dGTP(*anti*) that forms a stable hydration shell within hydrogen bonding distance to the adducted oxygen. Consequently, this metal helps alleviate the clash at O8 and permits binding of 8-oxo-dGTP*(anti)* without repositioning Pα. A similar phenomena is observed in the 8-oxo-dGTP*(syn)* conformation, where the exocyclic N2 forms an intramolecular hydrogen bond with Pα, stabilizing good nascent base pair geometry. This implies that the interaction of Pα by either N2 or a divalent metal cation is a hallmark characteristic of 8-oxo-dGTP insertion during both mutagenic and non-mutagenic insertion, respectively.

Damaged substrates complicate the ability of DNA polymerases to select the correct nucleotide[23-25]. Structural studies have identified that correct and incorrect non-damaged nucleotides are discriminated from each other based on proper alignment of catalytic atoms. The planar nature of 8-oxo-dGTP places O3' of the primer terminus near Pα so that only minor structural rearrangements are needed for nucleotidyl transfer. Following insertion of a correct nucleotide results in a stable ternary product complex, while incorrect insertion promotes rapid re-opening of the enzyme[26]. Immediately following 8-oxo-dGTP insertion the polymerase reopened, similar to an incorrect insertion and implying 8-oxo-dGMP promotes instability. These findings show that 8-oxo-dGTP utilizes characteristics of both correct and incorrect insertion elements.

Recent structural studies have identified a transient third metal binding site associated with the products[26,27]. For pol β, this third metal (Mg_p) was only observed in the product complex following insertion of the correct, but not incorrect, nucleotide. The appearance of the product metal was unexpected following 8-oxo-dGTP(*syn*) misinsertion opposite Ad, but consistent with the good base pair geometry exhibited by this mispair. It appears that these adjunct metal sites are necessary to neutralize negative charge that may be inherent in the substrate or that transiently develops during chemistry.

We can infer a mechanistic model for the role of these adjunct metal ions during catalysis (Fig. 4c). In the pre-catalytic GS the primer terminus, Mg_c, Mg_n, and incoming nucleotide are bound. Deprotonation of O3' initiates nucleophilic attack at Pα and as O3' approaches Pα it sterically clashes with the non-bridging oxygens of Pα. This results in a transition state and localized charges on O3', Pα, and $O_{Pα}$ that recruit a metal ion to polarize Pα, thus facilitating O3' attack by making Pα more positive and $O_{Pα-β}$ more negative. Such a role has been postulated for a basic side chain in A- and B-family DNA polymerases[28]. The accumulating negative charge on $O_{Pα-β}$ also promotes protonation of PP_i, which has been proposed to be a key rate-limiting step[29]. Following product formation this metal could transfer to the nearby product metal binding site, while the catalytic metal rapidly dissociates due to the lose of a coordinating ligand (O3'). Accordingly, the appearance/disappearance of cations around the active site represents an elegant ballet of electrons during DNA synthesis.

The structures captured here reveal how 8-oxo-dGTP escapes general polymerase discrimination checkpoints by modulating the highly charged DNA polymerase active site. Importantly, if 8-oxo-dGTP were to be inserted into a single-nucleotide gap, DNA ligase would be responsible for sealing the nick with a modified base pair. Abnormalities at the nick would hasten abortive ligation and stabilize the cytotoxic nick, thus increasing the probability for apoptotic cell signaling[30]. Similarly, the extension efficiency during error-free DNA synthesis from the modified base pair would be reduced (*i.e.*, DNA synthesis would pause), promoting the generation of cytotoxic strand breaks. Therefore, the insertion and subsequent processing of 8-oxo-G in DNA offers a mechanism to manipulate the oxidative DNA damage response as well as target cancer cells that have an elevated metabolic rate.

METHODS SUMMARY

DNA sequences

To generate the 16-mer the following DNA sequences were used for crystallization (coding nucleotide is underlined): template, 5'-CCG ACA/C GCG CAT CAG C-3'; primer, 5'-GCT GAT GCG C-3'; downstream, 5'-GTC GG-3'. The downstream sequence was 5'-phosphorylated. The kinetic studies required extending the downstream and upstream sequences to employ a 34-mer DNA substrate. The sequence of the template strand was 5'-GTA CCC GGG GAT CCG TAC A/CGC GCA TCA GCT GCA G -3'. The underlined A/C represents the coding nucleotide as either an Ad or Cy. DNA substrates for single-nucleotide gap filling DNA synthesis measurements were prepared by annealing three purified oligonucleotides. Each oligonucleotide was suspended in 10 mM Tris-HCl, pH 7.4, and 1 mM EDTA and the concentration was determined from their UV absorbance at 260 nm. The annealing reactions were carried out by incubating a solution of primer with downstream and template oligonucleotides (1:1.2:1.2 molar ratio, respectively) at 95 °C for 5 min followed by 65 °C for 30 min and finally cooling 1 °C/min to 10 °C in a PCR thermocycler.

Protein expression, crystallization and structural determination

Human wild-type, R283A, and R283K DNA polymerase β were overexpressed in *E. coli* and purified as described previously[31]. Binary complex crystals with a templating cytosine or adenine in a 1-nt gapped DNA were grown as previously described[18]. The time-lapse crystallography was performed as previously described and is briefly summarized here[26]. Binary pol β:DNA complex crystals were first transferred to a cryosolution containing 15% ethylene glycol, 50 mM imidazole, pH 7.5, 20% PEG3350, 90 mM sodium acetate, 3 mM 8-oxodGTP or dGTP, and 50 mM $CaCl_2$ for 1 h. These ground state (GS) ternary complex crystals were then transferred to a cryosolution containing 200 mM $MgCl_2$ or $MnCl_2$ for varying times. All reactions were stopped by freezing the crystals at 100K prior to data collection at the home source, 1.54 Å, or the Advanced Photon Source, 1.0 Å (Argonne National Laboratory). In house data collection was done on a SATURN92 CCD detector system mounted on a MiraMax-007HF rotating anode generator at a wavelength of 1.54 Å. This allows for anomalous data detection after phasing by molecular replacement. Remote data collection was done at Southeast Regional Collaborative Access Team (SER-CAT) BM-22 beamline at the Advanced Photon Source (Argonne National Laboratory) at a wavelength of 1.0 Å, with the MAR225 area detector. Data were processed and scaled using the HKL2000 software package[32]. Initial models were determined using molecular replacement with the open binary (3ISB) or closed ternary (2FMS) structures of pol β and all R_{free} flags were taken from the starting model. Refinement was carried out using PHENIX and model building using Coot[33,34]. The metal-ligand coordination restraints were generated by ReadySet (PHENIX) and not utilized until the final rounds of refinement. Partial catalysis models were generated with both the reactant and product species and occupancy refinement was performed. The figures were prepared in PyMol and all density maps were generated after performing simulated annealing[35]. Ramachandran analysis determined 100% of nonglycine residues lie in allowed regions and at least 97% in favored regions.

Kinetic characterization

Steady-state kinetic parameters for single-nucleotide gap filling reactions with wild-type enzyme were determined by initial velocity measurements as described previously[36]. Unless noted otherwise, enzyme activities were determined using a standard reaction mixture containing 50 mM Tris-HCl, pH 7.4 (37 °C), 100 mM KCl, 10 mM $MgCl_2$, 1 mM dithiothreitol, 100 μg/ml bovine serum albumin, 10% glycerol, and 200 nM single-nucleotide gapped DNA. Enzyme concentrations and reaction time intervals were chosen so that substrate depletion or product inhibition did not influence initial velocity measurements. Due to the low activity of the Arg283 mutants (alanine and lysine), the catalytic efficiencies were determined by single-turnover analysis as described before except that the enzyme/DNA ratio was 10 [37]. Reactions were quenched with 0.3 M EDTA and mixed with an equal volume of 95% formamide dye. The substrates and products were separated on 16% denaturing (8 M urea) polyacrylamide gels. Since a 6-carboxyfluorescein 5'-labeled primer was used in these assays, the substrates and products were quantified using a GE Typhoon 8600 phosphorimager in fluorescence mode (532 nm laser, 526 short pass filter). Kinetic parameters were determined by fitting the rate data to a hyperbolic equation. When the observed rates could not be saturated owing to weak substrate binding, the data were fitted to an alternate form of the equation to extract catalytic efficiency (k_{cat}/K_M, best-fit initial slope). $k_{obs} = ((k_{cat}/K_M) * [S]) / (1 + ([S]/K_M))$ The mean and standard error of at least two independent determinations are illustrated in plots that highlight substrate discrimination.

Quantum mechanical analysis

The three systems are shown in Extended Data Figure 4 and described here. They are (1) 8-oxoGTP*(anti)* with the Ca_c, Ca_n, Ca_g ions, the coordinating 8 water molecules, and the three acetate ions (mimicking Asp190, 192, and 256 of pol β); (2) all atoms in system 1 except for the Ca_g and its coordinating water molecules; (3) dGTP*(anti)* with the Ca_c, Ca_n, Ca_g ions, the coordinating 8 water molecules, and the three acetate ions (mimicking Asp190, 192, and 256 of pol β). The base of 8-oxoGTP was optimized under minimum constraints to keep the geometries closer to the crystallographic structure at the B3LYP level of theory with the 6-31+g* basis set using the program Gaussian09.D01[38]. All charges were calculated using the ChelpG procedure in Gaussian09.D01 at the 6-31++g** basis set level[39].

Molecular dynamics simulations

Two reference systems were simulated by MD for 80 ns. System 1 was prepared using the entire GS 8-oxodGTP*(anti)*:Cy crystal structure (0 s). It consists of the DNA, 8-oxodGTP*(anti)*, pol β, 302 crystal water molecules, and three Mg^{2+} ions that replace the Ca^{2+} ions in the crystal structure at the catalytic, nucleotide, and ground metal binding sites. System 2 was prepared as system 1, but with 8-oxodGTP replaced by dGTP*(anti)*. For all structures, missing atoms were added using CHARMM[40], and the disordered residues 1-10 of polymerase were attached by Accelrys Discovery Studio. Both systems were solvated with TIP3P water molecules. The smallest image distance between the solute and the faces of the periodic cubic cell is set to 12 Å. The total number of water atoms is 49089 and total number of atoms is 55521. Neutralizing ions (Na^+) and 150 mM NaCl were added to both

systems. All of the Na^+ and Cl^- ions were placed at least 8 Å away from each other, pol β, and the DNA. Both systems were minimized with fixed positions for all heavy atoms of pol β and DNA for 10,000 steps. The equilibration process was started with a 200 ps simulation at 300K using Langevin dynamics, while keeping all the heavy atoms of pol β and DNA fixed. This was followed by unconstrained minimization consisting of 20,000 steps. The systems were then equilibrated for 500 ps at constant pressure and temperature. Pressure was maintained at 1 atm using the Langevin piston method[41]. The temperature was maintained at 300K using weakly coupled Langevin dynamics of nonhydrogen atoms with a damping coefficient of 10 ps^{-1}. The systems were simulated in periodic boundary conditions with full electrostatics computed using the particle mesh Ewald (PME) method[42]. Short-range nonbonded terms were evaluated at every step using a 12 Å cutoff for van der Waals interactions and a smooth switching function. The production simulations were performed for 80 ns with a 2 fs timestep. The minimization, equilibration, and production MD simulations were performed by NAMD simulation package[43] with the CHARMM27 all-atom force field [44-46]. The force field parameters for 8-oxoG were adopted from earlier works[47,48]. The average distances and standard deviations are calculated using MD trajectories in the 50-80 ns time range.

Extended Data

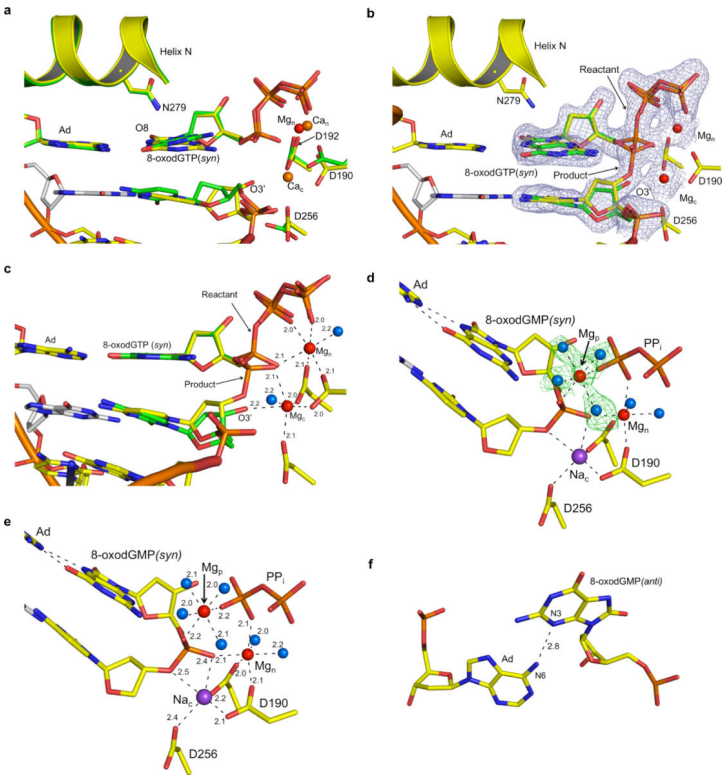

Extended Data Figure 1. Mutagenic 8-oxo-dGTP insertion opposite adenine

a, Overlay of the ternary complex for 8-oxo-dGTP*(syn)*:Ad generated with Ca^{2+} or a dideoxy-terminated primer (PDB ID 3MBY) is shown in yellow and green, respectively (RMSD of 0.17 Å). **b,** The pol β active site is shown with a $2F_o$-F_c map contoured at 1.5σ

after a 20 s soak. Key active site residues are indicated and Mg^{2+} ions are shown as red spheres. The reactant 8-oxo-dGTP and product 8-oxo-dGMP are shown in green and yellow respectively. **c,** A focused view of panel **b** with the density removed. Coordinating waters (blue) and their distances (Å) to active site metals are shown. **d,** The active site following a 40 s soak is shown with an omit map (3σ) for the Mg_p and coordinating waters. **e,** The coordination distances (Å) for the Na_c, Mg_p, and Mg_n metals are indicated for the closed product complex after a 40 s soak. **f,** The 8-oxodGMP*(anti)*:Ad contact between N3 and N6 of 8-oxo-dGMP and Ad respectively is shown for the open product complex after a 90 s soak.

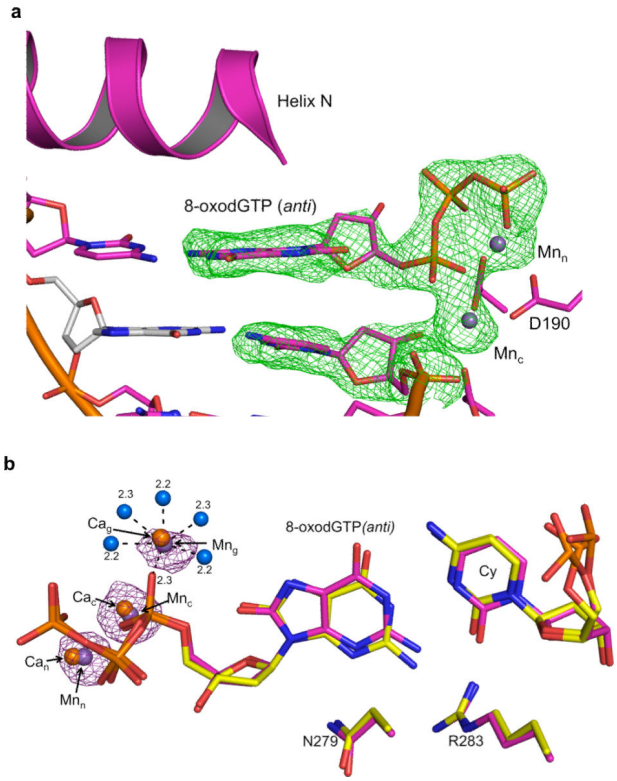

Extended Data Figure 2. Pre-catalytic GS with 8-oxo-dGTP and templating cytosine after a 5 s soak in $MnCl_2$

a, The pre-catalytic pol β active site is shown with an omit map (3σ). The ground state metal (Mn_g) has been removed for clarity. **b,** The view is a 90° rotation relative to panel **a**. An overlay of the 8-oxo-dGTP*(anti)* with Ca^{2+} and Mn^{2+} is shown in yellow and purple respectively. The anomalous density map contoured at 5σ for the Mn^{2+} ions is shown in purple. The Mn_g coordinating water molecules are shown in blue and the distances (Å) are indicated.

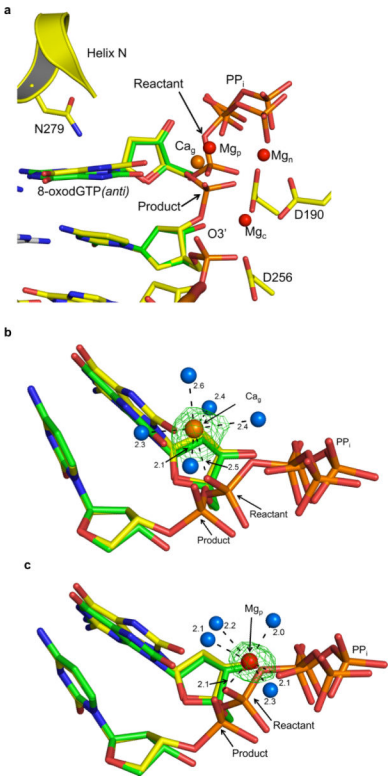

Extended Data Figure 3. Reaction with 8-oxo-dGTP opposite templating cytosine

a, Focused view of the active site following a 40 s soak is shown with key residues indicated; density has been removed for clarity (see Fig. 2e for density). **b,** An omit map (3σ) for Ca_g is shown. Coordinating waters are shown in blue (distances, Å). **c,** An omit map (3σ) for Mg_p is shown.

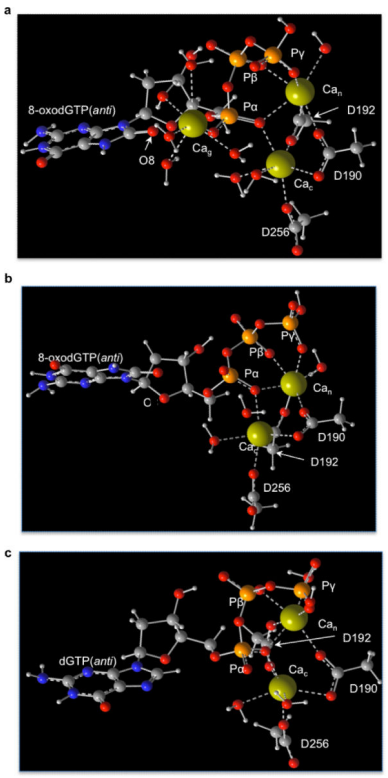

Extended Data Figure 4. QM computational models for 8-oxo-dGTP(anti) and dGTP(anti)

The models used for the QM computational studies with the calcium ions, oxygen, phosphates, carbon, nitrogen, and protons shown in green, red, orange, grey, blue, and white, respectively. The key atoms and Asp190, Asp192, and Asp256 mimics are indicated. **a,** The 8-oxo-dGTP*(anti)* with 3 calcium ions and 8 water molecules. **b,** The 8-oxo-dGTP*(anti)* with 2 calcium ions and 3 water molecules. **c,** The dGTP*(anti)* with 2 calcium ions and 3 water molecules.

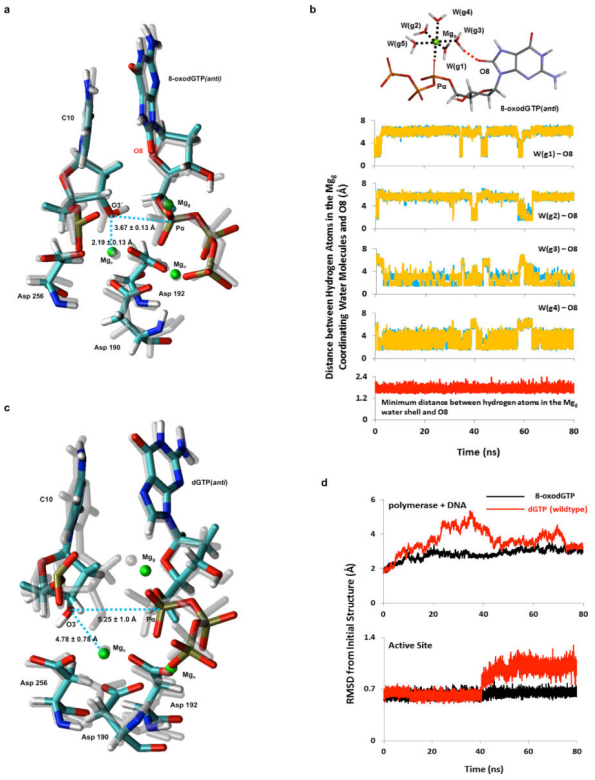

Extended Data Figure 5. MD simulation analysis of 8-oxo-dGTP*(anti)* and dGTP*(anti)* opposite Cy

a, The 8-oxo-dGTP*(anti)* opposite Cy at 80 ns superimposed upon the initial structure. A multicolor code based on atom type is used for the final MD structure, whereas the reference initial structure is shown in light grey. The catalytic (Mg_c), nucleotide (Mg_n), and ground (Mg_g) magnesium metal ions are shown in green, and average distances over the course of the simulation are indicated for Pα-O3' and Mg_c-O3'. **b,** Distance distributions between hydrogen atoms in the water shell and O8 in the 8-oxo-dGTP*(anti)*:Cy simulation. A snapshot of the 8-oxo-dGTP, Mg_g and water shell (W(g1-g5)) is plotted at top. Black and red dotted lines indicate Mg_g coordination and a hydrogen-bonding interaction between a water molecule and O8, respectively. Four of the five water molecules in the water shell (W(g1-g4)) contribute to hydrogen-bonding interactions with O8. Blue and orange lines indicate distances between hydrogen atoms in each water molecule and O8. The red line in the bottom plot indicates the minimum distance between hydrogen atoms in the water shell and O8. **c,** The dGTP*(anti)* opposite Cy at 80 ns superimposed upon the initial structure (grey). Distances and ion labeling are as for a. **d,** RMSD of the evolving MD structure for the entire polymerase/DNA complex (top) and for the active site only (bottom), with respect to the crystal structure.

Extended Data Table 1

Data collection and refinement statistics of pol β 8-oxo-dGTP insertion opposite adenine.

	0 s Ground state	20 s Reactant state	40 s Product state	90 s Product state
Templating Base	Adenine	Adenine	Adenine	Adenine
Data Collection				
Wavelength	1.00	1.00	1.00	1.00
Space group	$P2_1$	$P2_1$	$P2_1$	$P2_1$
Cell dimensions				
a, *b*, *c* (Å)	50.9,79.9,55.5	50.8,79.9,55.4	50.9,80.4,55.4	55.1,80.8,55.5
a, *b*, *g* (°)	90,107.6,90	90,107.6,90	90,107.7,90	90,109.6,90
Resolution (Å)	50.0-1.90	50.0-1.88	50.0-1.98	50.0-2.35
R_{sym} or R_{merge} [*] (%)	6.8 (52.8)	5.5 (34.2)	6.0 (28.4)	5.2 (33.4)
/Is/	28.9 (4.4)	23.3 (2.3)	24.2 (2.8)	24.3 (2.3)
Completeness (%)	98.0 (97.7)	95.6 (68.9)	96.6 (72.1)	97.3 (77.0)
Redundancy	5.7 (4.0)	3.3 (1.8)	3.5 (2.3)	3.5 (2.5)
Refinement				
Resolution (Å)	1.90	1.88	1.98	2.35
No. reflections	57079	56411	51562	34952
R_{work}/ R_{free}	17.5/23.2	17.4/21.4	17.7/23.9	20.8/26.4
No. atoms				
Protein	2677	2673	2673	2593
DNA	659	681	681	681
Water	341	278	274	86
B-factors (Å^2)				
Protein	25.9	29.2	26.2	40.5
DNA/8oxo/PP_1	26.2/18.7/-	36.5/18.2/25.1	35.0/20.9/28.1	38.2/57/-
Water	27.8	33.1	31.57	30.4
R.m.s deviations				
Bond length (Å)	0.01	0.01	0.01	0.01
Bond angles (°)	1.20	1.00	1.09	1.16
Reaction Ratio				
Pol β conformation	closed	closed	closed	open
Ratio of RS/PS[†]	1.0/0	0.4/0.6	0/1.0	0/1.0
Occupancy				
Metal C/N/G/P[‡]	1.0/1.0/-/-	1.0/1.0/-/-	-/1.0/-/0.7	-
PP_1	-	0.6	1.0	-
PDB ID	4UAW	4UAZ	4UAY	4UB1

[*] Highest resolution shell is shown in parentheses.

[†] RS and PS represent the reactant state and product states, respectively.

[‡] Metal C/N/G/P refers to the catalytic, nucleotide, ground, and product metal binding sites, respectively.

Extended Data Table 2

Key DNA and structural parameters near the pol β active site[*].

Complex	Sugar pucker		Buckle (NBP)[‡]	Shear (NBP)
	Primer[†]	Incoming		
dC–dGTP	C3′-endo	C3′-endo	8.5	−0.17
dC–8oxodGTP	C3′-endo	C4′-exo	−13.1	0.43
dA–8oxodGTP	C3′-endo	C3′-endo	0.7	0.03
dG–dATP[§]	C2′-endo	C3′-endo	43.2	0.61
dA–8oxodGTP[II]	C2′-endo	C4′-exo	−13.9	−0.06

[*] Parameters extracted with 3DNA

[†] Primer Terminus

[‡] Nascent Base Pair

[§] PDB ID 4LVS

[II] PDB ID 3MBY

Extended Data Table 3

Data collection and refinement statistics of pol β insertion opposite cytosine with 8-oxo-dGTP and dGTP.

	0 s Ground state	40 s Reactant state	60 s Product State	120 s Product state	5 s ($MnCl_2$) Ground state	0 s (dGTP) Ground state
Templating Base	Cytosine	Cytosine	Cytosine	Cytosine	Cytosine	Cytosine
Data Collection						
Wavelength	1.51	1.00	1.54	1.54	1.54	1.54
Space group	$P2_1$	$P2_1$	$P2_1$	$P2_1$	$P2_1$	$P2_1$
Cell dimensions						
a, *b*, *c* (Å)	50.7,79.8,55.5	50.8,79.8,55.6	50.7,80.1,55.4	55.1,79.6,55.7	55.1,77.7,55.1	50.6,79.4,55.5
a, *b*, *g* (°)	90,107.5,90	90,107.6,90	90,107.8,90	90,109.7,90	90,114.2,90	90,107.5,90
Resolution (Å)	50.0-1.96	50.0-1.85	50.0-2.06	50.0-2.51	50.0-2.15	50.0-1.96
R_{sym} or R_{merge} (%)	6.0 (42.1)	5.4 (27.5)	8.3 (51.1)	7.6 (62.3)	6.9 (51.6)	6.8 (51.3)
/*I*s/	20.4 (2.1)	20.9 (2.9)	16.3 (2.1)	17.6 (2.2)	13.3 (2.3)	19.6 (2.2)
Completeness (%)	98.4 (87.7)	98.1 (79.0)	97.4 (91.2)	99.5 (99.7)	99.6 (99.5)	99.5 (95.8)
Redundancy	3.0 (1.7)	3.2 (1.9)	4.7 (3.3)	3.6 (3.5)	3.2 (2.9)	4.8 (2.3)
Refinement						
Resolution (Å)	2.0	1.90	2.06	2.51	2.15	1.96
No. reflections	51032	63741	21786	25631	39111	49693
R_{work}/ R_{free}	18.2/25.1	17.6/22.3	19.1/25.2	20.5/27.5	21.2/27.4	17.9/22.8
No. atoms						
Protein	2673	2673	2673	2593	2673	2674
DNA	627	661	661	661	627	627
Water	304	293	172	63	101	235
B-factors (Å^2)						
Protein	27.7	28.8	32.3	38.9	42.1	36.1

	0 s Ground state	40 s Reactant state	60 s Product State	120 s Product state	5 s ($MnCl_2$) Ground state	0 s (dGTP) Ground state
DNA/8oxo/PP_1	36.6/18.8/-	38.0/21.0/20.5	41.4/25.8/28.1	34.8/65.4/-	44.1/38.3/-	42.6/25.0/-
Water	29.4	39.5	30.0	20.0	31.4	32.8
R.m.s deviations						
Bond length (Å)	0.01	0.01	0.006	0.01	0.007	0.009
Bond angles (°)	1.17	1.08	1.20	1.26	1.1	1.17
Reaction Ratio						
Pol β conformation	closed	closed	closed	open	closed	closed
Ratio of RS/PS†	1.0/0	0.6/0.1	0/1.0	0/1.0	1.0/0	1.0/0
Occupancy						
Metal C/N/G/P‡	1.0/1.0/1.0/-	1.0/1.0/0.6/0.4	-/1.0/-/0.6	-	1.0/1.0/1.0/-	1.0/1.0/-/-
PP	-	0.1	1.0	-	-	-
PDB ID	4UBC	4UBB	4UB3	4UB2	4UB5	4UB4

*Highest resolution shell is shown in parentheses.

†RS and PS represent the reactant state and product states, respectively.

‡Metal C/N/G/P refers to the catalytic, nucleotide, ground, and product metal binding sites, respectively.

Extended Data Table 4

QM point charges for each atom of 8-oxo-dGTP*(anti)* and dGTP*(anti)* with either 2 or 3 calcium ions

The MD point charges used with three magnesium ions are shown for reference in the last column. The units are in electron charge (e) and the key is shown for reference.

Number*	Atom	8-oxodGTP 3 metals	8-oxodGTP 2 metals	dGTP 2 metals	8-oxodGTP (MD)
1	H	0.41	0.39	0.4	N/A
2	O	−0.67	−0.74	−0.68	−0.9
3	P	1.49	1.4	1.42	1.10
4	O	−0.9	−0.82	−0.87	−0.9
5	O	−0.83	−0.84	−0.82	−0.9
6	O	−0.62	−0.56	−0.58	−0.86
7	P	1.49	1.33	1.32	1.50
8	0	−0.81	−0.83	−0.79	−0.82
9	0	−0.88	−0.89	−0.82	−0.82
10	0	−0.75	−0.41	−0.51	−0.74
11	P	1.44	1.32	1.33	1.5
12	0	−0.91	−0.86	−0.91	−0.82
13	O	−0.97	−0.89	−0.77	−0.82
14	O	−0.22	−0.17	−0.33	−0.62
15	C	0.03	0.01	0	−0.08
16	H	0.11	0.06	0.14	0.09
17	H	0.05	0.04	0.05	0.09
18	C	0.14	0.25	0.13	0.16

Number *	Atom	8-oxodGTP 3 metals	8-oxodGTP 2 metals	dGTP 2 metals	8-oxodGTP (MD)
19	H	0.03	−0.04	0.02	0.09
20	C	0.63	0.68	0.72	0.14
21	H	−0.12	−0.08	−0.14	0.09
22	0	−0.82	−0.88	−0.85	−0.66
23	H	0.48	0.49	0.49	0.43
24	C	−0.16	−0.16	−0.20	−0.18
25	H	0.05	0.01	0.01	0.09
26	H	−0.01	−0.02	0.04	0.09
27	C	0.59	0.60	0.44	0.16
28	H	−0.05	−0.08	0.02	0.09
29	0	−0.55	−0.58	−0.55	−0.5
30	N	−0.24	−0.26	−0.14	0.16
31	C	0.66	0.71	0.33	0.41
32 †	O/H	−0.63	−0.61	0.08	−0.64
33	N	−0.51	−0.54	−0.57	−0.34
34 ‡	H	0.37	0.38	–	0.38
35	C	−0.19	−0.18	−0.02	0
36	C	0.77	0.77	0.78	0.33
37	O	−0.62	−0.66	−0.63	−0.58
38	N	−0.81	−0.83	−0.88	−0.23
39	H	0.42	0.41	0.42	0.32
40	C	0.91	0.92	0.97	0.57
41	N	−0.86	−0.89	−0.88	−0.87
42	H	0.38	0.37	0.36	0.41
43	H	0.36	0.35	0.33	0.42
44	N	−0.72	−0.72	−0.78	−0.57
45	C	0.44	0.43	0.39	0.23

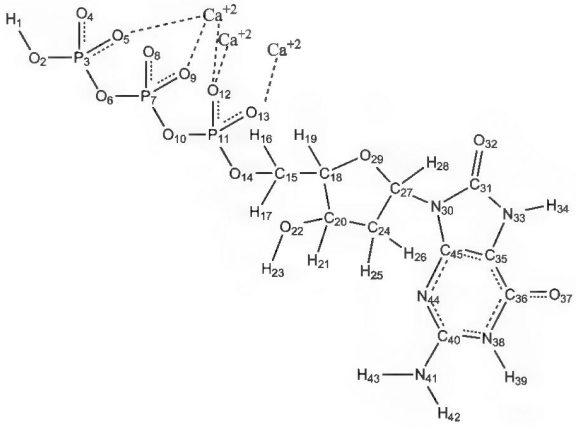

* The position of each atom is shown in the chemical structure cartoon below the table.

† The oxygen or proton corresponds to 8-oxodGTP and dGTP respectively.

‡Proton corresponds to 8-oxodGTP only.

Extended Data Table 5

Average distances in the active sites in 8-oxo-dGTP*(anti)* and dGTP*(anti)*

W(c), W(n), W(g1-g5) are water molecules bound to the Mg_c, Mg_n and Mg_g, respectively. The Mg_c in the dGTP*(anti)* system establishes a new coordination with a water molecular (W(c)*) after 40 ns. The average values are calculated using 50-80 ns range of MD trajectories.

Distance	8-oxodGTP (Å)	dGTP (Å)
Mg_c–OD2 (ASP190)	1.81 ± 0.04	1.81 ± 0.04
Mg_c–OD1 (ASP192)	1.80 ± 0.04	1.81 ± 0.04
Mg_c–OD2 (ASP256)	1.80 ± 0.04	1.81 ± 0.04
Mg_c–O1A (Pα)	3.18 ± 0.13	3.34 ± 0.25
Mg_c- O3' (C10)	2.19 ± 0.13	4.78 ± 0.42
Mg_c– W(c)	1.95 ± 0.05	2.00 ± 0.07
Mg_c–W(c)*	N/A	1.98 ± 0.07
Pa – O3' (C10)	3.87 ± 0.13	5.25 ± 1.01
Mg_n– OD1 (ASP190)	1.88 ± 0.05	1.86 ± 0.05
Mg_n– OD2 (ASP192)	1.87 ± 0.05	1.88 ± 0.06
Mg_n– O1A (Pα)	1.90 ± 0.06	1.92 ± 0.06
Mg_n– O2B (Pβ)	1.90 ± 0.06	1.91 ± 0.06
Mg_n– O3G (Pγ)	1.85 ± 0.05	1.84 ± 0.05
Mg_n–W(n)	2.00 ± 0.06	2.03 ± 0.07
Mg_g– O2A (Pα)	1.82 ± 0.04	1.82 ± 0.04
Mg_g– W(g1)	1.98 ± 0.06	1.99 ± 0.06
Mg_g–W(g2)	1.98 ± 0.06	1.99 ± 0.06
Mg_g– W(g3)	2.00 ± 0.07	1.99 ± 0.06
Mg_g– W(g4)	2.00 ± 0.07	2.01 ± 0.07
Mg_g– W(g5)	1.99 ± 0.07	1.98 ± 0.06
W(g)–O8 (8-oxodGTP)	1.73 ± 0.11	N/A
W(g) – N7 (dGTP)	N/A	3.9 ± 0.34 Å

Acknowledgments

We thank the Collaborative Crystallography group at NIEHS for help with data collection and analysis. We thank L. Pedersen for valuable discussions. Use of the advanced Photon Source was supported by the U.S. Department of Energy, Office of Science, Office of Basic Energy Sciences, under contract W-31-109-Eng-38. This research was supported by the Intramural Research Program of the NIH, National Institute of Environmental Health Sciences (project numbers Z01-ES050158 (S.W.), Z01-ES050161 (S.W.), and ZIC-ES043010 (L.P.)) and in association with the National Institutes of Health grant 1U19CA105010.

References

1. Reuter S, Gupta SC, Chaturvedi MM, Aggarwal BB. Oxidative stress, inflammation, and cancer: How are they linked? Free Radic. Biol. Med. 2010; 49:1603–1616.

2. Bont RD, Larebeke N. Endogenous DNA damage in humans: a review of quantitative data. Mutagenesis. 2004; 19:169–185. [PubMed: 15123782]

3. Fraga CG, Shigenaga MK, Park JW, Dega P, Ames BN. Oxidative damage to DNA during aging:8-hydroxy-2′-deoxyguanosine in rat organ DNA and urine. Proc. Natl. Acad. Sci. 1990; 87:4533–4537. [PubMed: 2352934]

4. Topal MD, Baker MS. DNA precursor pool: a significant target for N-methyl-N-nitrosourea in C3H/10T1/2 clone 8 cells. Proc. Natl. Acad. Sci. 1982; 79:2211–2215. [PubMed: 6954535]

5. Huber KV, et al. Stereospecific targeting of MTH1 by (S)-crizotinib as an anticancer strategy. Nature. 2014; 508:222–227. [PubMed: 24695225]

6. Gad H, et al. MTH1 inhibition eradicates cancer by preventing sanitation of the dNTP pool. Nature. 2014; 508:215–221. [PubMed: 24695224]

7. Foti JJ, Devadoss B, Winkler JA, Collins JJ, Walker GC. Oxidation of the guanine nucleotide pool underlies cell death by bactericidal antibiotics. Science. 2012; 336:315–319. [PubMed: 22517853]

8. Shibutani S, Takeshita M, Grollman AP. Insertion of specific bases during DNA synthesis past the oxidation-damaged base 8-oxodG. Nature. 1991; 349:431–434. [PubMed: 1992344]

9. Colussi C, et al. The Mammalian Mismatch Repair Pathway Removes DNA 8-oxodGMP Incorporated from the Oxidized dNTP Pool. Curr. Biol. 2002; 12:912–918. [PubMed: 12062055]

10. Pursell ZF, McDonald JT, Mathews CK, Kunkel TA. Trace amounts of 8-oxo-dGTP in mitochondrial dNTP pools reduce DNA polymerase γ replication fidelity. Nucl. Acids Res. 2008; 36:2174–2181. [PubMed: 18276636]

11. Oda Y, et al. NMR studies of a DNA containing 8-hydroxydeoxyguanosine. Nucl. Acids Res. 1991; 19:1407–1412. [PubMed: 2027747]

12. Amouroux R, Campalans A, Epe B, Radicella JP. Oxidative stress triggers the preferential assembly of base excision repair complexes on open chromatin regions. Nucl. Acids Res. 2010; 38:2878–2890. [PubMed: 20071746]

13. Cabelof DC, Raffoul JJ, Yanamadala S, Guo Z, Heydari AR. Induction of DNA polymerase ß-dependent base excision repair in response to oxidative stress in vivo. Carcinogenesis. 2002; 23:1419–1425. [PubMed: 12189182]

14. Beard WA, Wilson SH. Structure and mechanism of DNA polymerase β. Biochemistry. 2014; 53:2768–2780. [PubMed: 24717170]

15. Donigan KA, et al. Human POLB gene is mutated in high percentage of colorectal tumors. J. Biol. Chem. 2012; 287:23830–23839. [PubMed: 22577134]

16. Beese LS, Steitz TA. Structural basis for the 3′-5′ exonuclease activity of Escherichia coli DNA polymerase I: A two metal ion mechanism. EMBO J. 1991; 10:25–33. [PubMed: 1989886]

17. Sawaya MR, Prasad P, Wilson SH, Kraut J, Pelletier H. Crystal structures of human DNA polymerase β complexed with gapped and nicked DNA: Evidence for an induced fit mechanism. Biochemistry. 1997; 36:11205–11215. [PubMed: 9287163]

18. Batra VK, et al. Magnesium induced assembly of a complete DNA polymerase catalytic complex. Structure. 2006; 14:757–766. [PubMed: 16615916]

19. Batra VK, et al. Mutagenic conformation of 8-oxo-7,8-dihydro-2′-dGTP in the confines of a DNA polymerase active site. Nat. Struct. Mol. Biol. 2010; 17:889–890. [PubMed: 20526335]

20. Miller H, Prasad R, Wilson SH, Johnson F, Grollman AP. 8-OxodGTP incorporation by DNA polymerase β is modified by active-site residue Asn279. Biochemistry. 2000; 39:1029–1033. [PubMed: 10653647]

21. Wang YL, Schlick T. Distinct energetics and closing pathways for DNA polymerase beta with 8-oxoG template and different incoming nucleotides. BMC Struct. Biol. 2007; 7:7. [PubMed: 17313689]

22. Freudenthal BD, Beard WA, Wilson SH. DNA polymerase minor groove interactions modulate mutagenic bypass of a templating 8-oxoguanine lesion. Nucl. Acids Res. 2013; 41:1848–1858. [PubMed: 23267011]

23. Brown JA, Duym WW, Fowler JD, Suo Z. Single-turnover kinetic analysis of the mutagenic potential of 8-oxo-7,8-dihydro-2'-deoxyguanosine during gap-filling synthesis catalyzed by human DNA polymerases λ and β. J. Mol. Biol. 2007; 367:1258–1269. [PubMed: 17321545]

24. Eckenroth BE, Fleming AM, Sweasy JB, Burrows CJ, Doublie S. Crystal Structure of DNA Polymerase β with DNA Containing the Base Lesion Spiroiminodihydantoin in a Templating Position. Biochemistry. 2014; 53:2075–2077. [PubMed: 24649945]
25. Koag MC, Min K, Lee S. Structural basis for promutagenicity of 8-halogenated guanine. J. Biol. Chem. 2014; 289:6289–6298. [PubMed: 24425881]
26. Freudenthal BD, Beard WA, Shock DD, Wilson SH. Observing a DNA polymerase choose right from wrong. Cell. 2013; 154:157–168. [PubMed: 23827680]
27. Nakamura T, Zhao Y, Yamagata Y, Hua Y.-j. Yang W. Watching DNA polymerase η make a phosphodiester bond. Nature. 2012; 487:196–201. [PubMed: 22785315]
28. Beard WA, Wilson SH. Structural insights into the origins of DNA polymerase fidelity. Structure. 2003; 11:489–496. [PubMed: 12737815]
29. Sucato CA, et al. DNA polymerase β fidelity: Halomethylene-modified leaving groups in pre-steady-state kinetic analysis reveal differences at the chemical transition state. Biochemistry. 2008; 47:870–879. [PubMed: 18161950]
30. Harris JL, et al. Aprataxin, poly-ADP ribose polymerase 1 (PARP-1) and apurinic endonuclease 1 (APE1) function together to protect the genome against oxidative damage. Hum. Mol. Genet. 2009; 18:4102–4117. [PubMed: 19643912]
31. Beard WA, Wilson SH. Purification and domain-mapping of mammalian DNA polymerase β. Meth. Enzymol. 1995; 262:98–107. [PubMed: 8594388]
32. Otwinowski Z, Minor W. Processsing of X-ray diffraction data collected in oscillation mode. Meth. Enzymol. 1997; 276:307–326.
33. Adams PD, et al. PHENIX: A comprehensive Python-based system for macromolecular structure solution. Acta Crystallogr., Sect. D. 2010; 66:213–221. doi:doi:10.1107/S0907444909052925. [PubMed: 20124702]
34. Emsley P, Cowtan K. Coot: model-building tools for molecular graphics. Acta Crystallogr., Sect. D. 2004; 60:2126–2132. [PubMed: 15572765]
35. Schrodinger LLC. The AxPyMOL Molecular Graphics Plugin for Microsoft PowerPoint, Version 1.0. 2010
36. Beard WA, Shock DD, Wilson SH. Influence of DNA structure on DNA polymerase β active site function: Extension of mutagenic DNA intermediates. J. Biol. Chem. 2004; 279:31921–31929. [PubMed: 15145936]
37. Beard WA, Shock DD, Yang X-P, DeLauder SF, Wilson SH. Loss of DNA polymerase β stacking interactions with templating purines, but not pyrimidines, alters catalytic efficiency and fidelity. J. Biol. Chem. 2002; 277:8235–8242. [PubMed: 11756435]
38. Frisch, MJ., et al. Gaussian 09, Revision D.01. Gaussian, Inc.; Wallingford, CT, USA: 2009.
39. Chirlian LE, Francl MM. Atomic charges derived from electrostatic potentials: A detailed study. J. Comput. Chem. 1987; 8:894–905.
40. Brooks BR, et al. CHARMM: A program for macromolecular energy, minimization, and dynamics calculations. J. Comput. Chem. 1983; 4:187–217.
41. Feller SE, Zhang Y, Pastor RW, Brooks BR. Constant pressure molecular dynamics simulation: The Langevin piston method. J. Chem. Phys. 1995; 103:4613–4621.
42. Darden T, York D, Pedersen L. Particle mesh Ewald: An N•log(N) method for Ewald sums in large systems. J. Chem. Phys. 1993; 98:10089–10092.
43. Phillips JC, et al. Scalable molecular dynamics with NAMD. J. Comput. Chem. 2005; 26:1781–1802. [PubMed: 16222654]
44. Foloppe N, MacKerell JAD. All-atom empirical force field for nucleic acids: I. Parameter optimization based on small molecule and condensed phase macromolecular target data. J. Comput. Chem. 2000; 21:86–104.
45. MacKerell AD, et al. All-Atom Empirical Potential for Molecular Modeling and Dynamics Studies of Proteins. J. Phys. Chem. B. 1998; 102:3586–3616. [PubMed: 24889800]
46. MacKerell AD, Banavali NK. All-atom empirical force field for nucleic acids: II. Application to molecular dynamics simulations of DNA and RNA in solution. J. Comp. Chem. 2000; 21:105–120.

47. Wang Y, Arora K, Schlick T. Subtle but variable conformational rearrangements in the replication cycle of Sulfolobus solfataricus P2 DNA polymerase IV (Dpo4) may accommodate lesion bypass. Protein Sci. 2006; 15:135–151. [PubMed: 16322565]

48. Pavelites JJ, Gao J, Bash PA, Mackerell AD. A molecular mechanics force field for NAD+, NADH, and the pyrophosphate groups of nucleotides. J. Comput. Chem. 1997; 18:221–239.

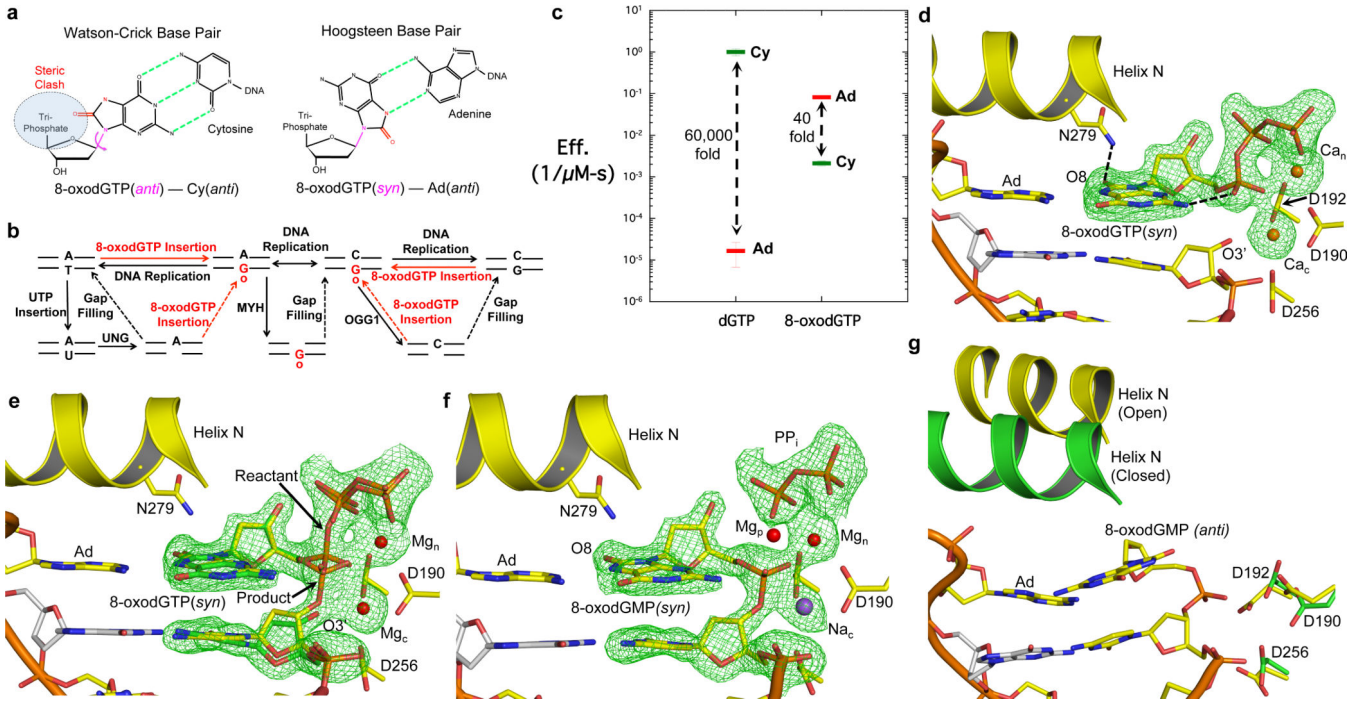

Figure 1. 8-oxodGTP specificity and insertion opposite adenine

a, 8-oxodGTP base pairing with Cy or Ad. **b,** Pathways associated with 8-oxoG DNA repair for the A to C transversion. Dashed lines are pol β insertion events. **c,** Pol β insertion efficiency of 8-oxodGTP and dGTP opposite either templating Cy or Ad. Discrimination for the preferred nucleotide is indicated. **d,** 8-oxodGTP*(syn)*:Ad pre-catalytic complex. **e,** Phosphodiester bond formation after a 20 s soak in $MgCl_2$ with the reactant (green) and product (yellow) states. **f,** Closed 8-oxodGMP:Ad product complex after a 40 s soak in $MgCl_2$. **g,** Open 8-oxodGMP:Ad product complex after a 90 s soak. Closed conformation is shown in green (PDB ID 2FMS). Fo-Fc maps (3σ) are in green. Ca^{2+}, Mg^{2+}, and Na^{+} are orange, red, and purple spheres respectively. The catalytic, nucleotide, and product metals are denoted with a subscript c, n, and p, respectively.

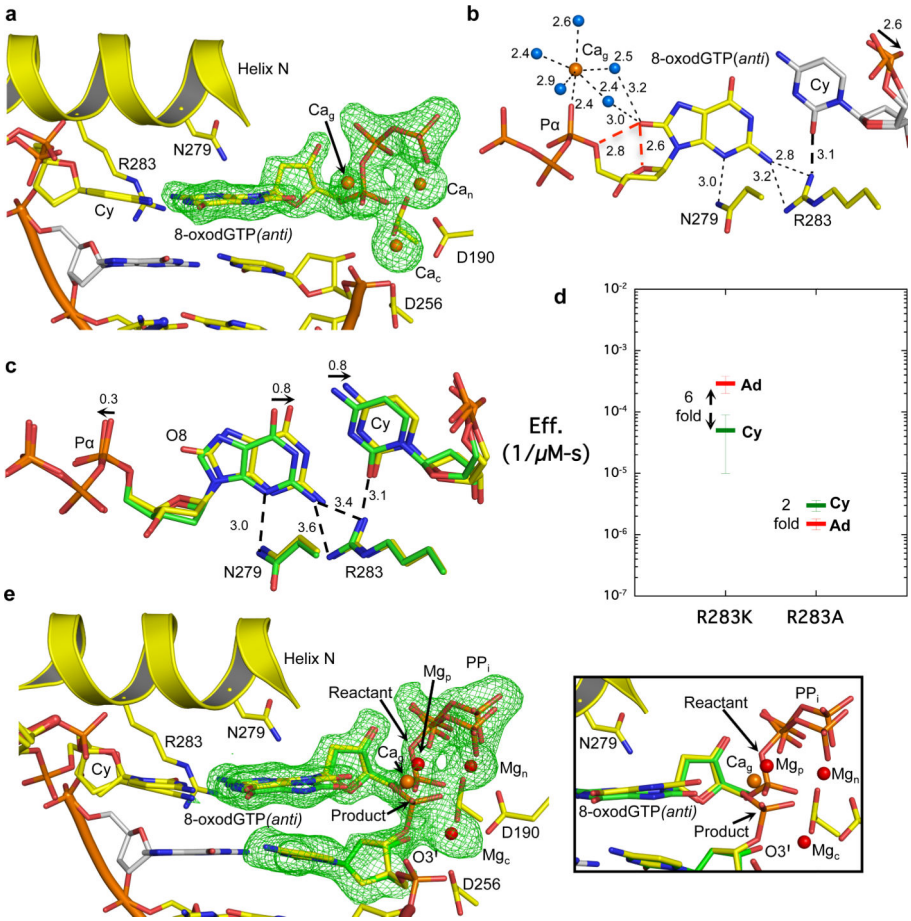

Figure 2. 8-oxodGTP insertion opposite cytosine

a, 8-oxodGTP:Cy pre-catalytic active site. **b,** A 90° rotation relative to panel a. Coordinating waters (blue) with distances (Å) are indicated. Clash at O8 is shown with red dashes. The Cy backbone shift is indicated. **c,** Overlay of 8-oxodGTP*(anti)* and dGTP*(anti)* opposite Cy is shown in yellow or green, respectively. The shift from the adducted O8 is indicated. **d,** Catalytic efficiency of 8-oxodGTP insertion opposite Cy or Ad for pol β R283K and R283A. **e,** The active site after a 40 s soak in $MgCl_2$ with the reactant (green) and product (yellow) species shown. A close-up without density is in the adjacent panel. Fo-Fc maps (3σ) are in green. Ca^{2+}, Mg^{2+}, and Na^{+} are orange, red, and purple spheres, respectively. The catalytic, nucleotide, ground, and product metals are denoted with a subscript c, n, g, and p, respectively.

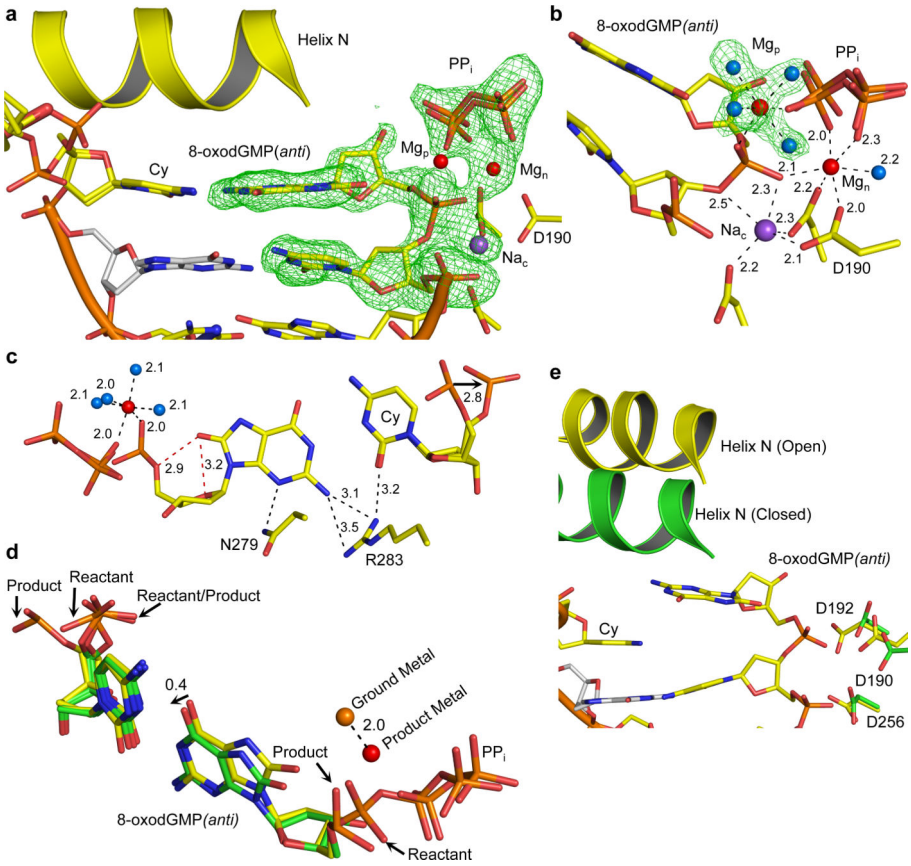

Figure 3. Product complex with 8-oxodGMP*(anti)*:Cytosine

a, Closed 8-oxodGMP:Cy product complex after a 60 s soak in $MgCl_2$. **b,** Active site of the closed 8-oxodGMP:Ad product complex with coordination distances (Å) and waters (blue). **c,** A 90° rotation relative to panel a. The clash at O8 is shown with red dashed lines. **d,** Overlay of the ground (green) and product (yellow) 8-oxodGTP*(anti)*:Cy complexes. The distance (Å) between the ground and product metal sites is shown with a dashed line. **e,** Open 8-oxodGMP:Cy product complex after a 120 s soak in $MgCl_2$. Closed conformation is shown in green (PDB ID 2FMS). Fo-Fc maps (3σ) are in green. Ca^{2+}, Mg^{2+}, and Na^{+} are orange, red, and purple spheres, respectively.

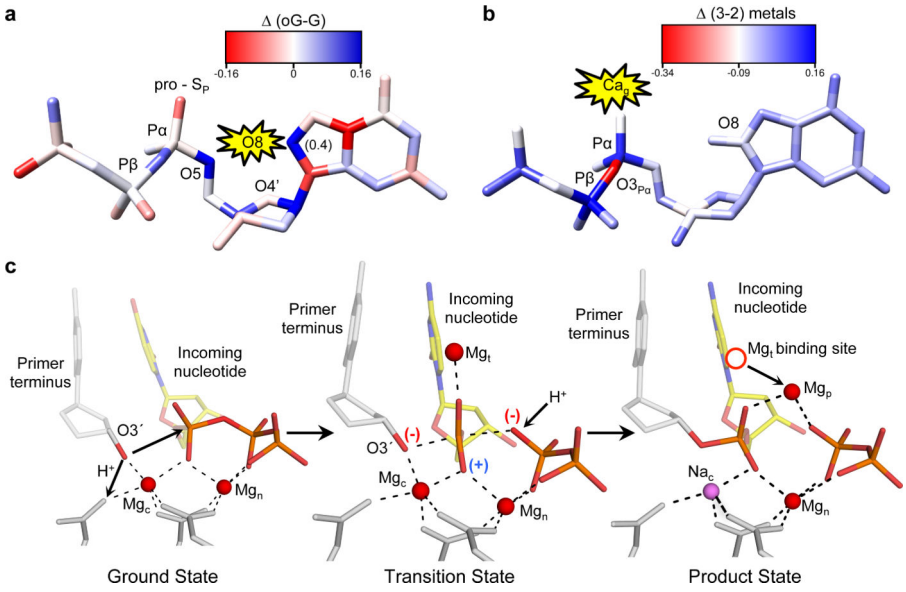

Figure 4. Charge modulation of the polymerase active site

a, The charge difference for each atom of dGTP*(anti)* and 8-oxodGTP*(anti)* is plotted onto dGTP with a color key shown. The only value that does not fall within the indicated range is C8 (0.4e). **b,** The charge difference for each atom of 8-oxodGTP*(anti)* with three and two metals is mapped onto 8-oxodGTP with a color key shown. **c,** Proposed model for the catalytic mechanism of nucleotide insertion. The primer terminus is shown in grey with O3′ in red and the incoming nucleotide in yellow. The transition state includes the catalytic (Mg_c), nucleotide (Mg_n), and transition (Mg_t) metals. The transition metal is in the same location as the previous GS metal binding site. The localized relative charges are indicated.